

Unified Spatio-Temporal Tri-Perspective View Representation for 3D Semantic Occupancy Prediction

Sathira Silva¹, Savindu Wannigama¹, Gihan Jayatilaka², Muhammad Haris Khan³, and Roshan Ragel¹

¹ University of Peradeniya, Peradeniya 20400, Sri Lanka
[e17331](mailto:e17331@eng.pdn.ac.lk), [e17369](mailto:e17369@eng.pdn.ac.lk), [roshanr](mailto:roshanr@eng.pdn.ac.lk)

² University of Maryland, College Park, MD 20742, USA
gihan@cs.umd.edu

³ Mohamed Bin Zayed University of AI, Abu Dhabi, UAE
muhhammad.haris@mbzuai.ac.ae

Abstract. Holistic understanding and reasoning in 3D scenes play a vital role in the success of autonomous driving systems. The evolution of 3D semantic occupancy prediction as a pretraining task for autonomous driving and robotic downstream tasks capture finer 3D details compared to methods like 3D detection. Existing approaches predominantly focus on spatial cues such as tri-perspective view embeddings (TPV), often overlooking temporal cues. This study introduces a spatiotemporal transformer architecture S2TPVFormer for temporally coherent 3D semantic occupancy prediction. We enrich the prior process by including temporal cues using a novel temporal cross-view hybrid attention mechanism (TCVHA) and generate spatiotemporal TPV embeddings (i.e. S2TPV embeddings). Experimental evaluations on the nuScenes dataset demonstrate a substantial 4.1% improvement in mean Intersection over Union (mIoU) for 3D Semantic Occupancy compared to TPVFormer, confirming the effectiveness of the proposed S2TPVFormer in enhancing 3D scene perception.

Keywords: Temporal Reasoning · Spatiotemporal Transformer · 3D Semantic Occupancy Prediction

1 Introduction

Accurate and comprehensive 3D scene understanding and reasoning are pivotal for the development of robotic and autonomous driving systems. This reasoning spans two critical aspects: spatial reasoning and temporal reasoning. In recent years, vision-centric 3D perception has gained significant interest as a promising alternative to LiDAR-based methods [18, 46, 31, 33] within the field of autonomous driving research. Vision-based approaches for 3D perception offer distinct advantages over LiDAR-based methods reliant on explicit depth measurements. Notably, vision-centric methods excel in identifying road elements,

such as traffic lights and road signs, a task that proves challenging for LiDAR-based approaches.

For an extended period, one of the most popular 3D perception tasks has been 3D object detection [35, 40, 23, 15], estimating the locations and dimensions of objects and producing concise 3D bounding boxes for downstream tasks. However, object detection methods are constrained in terms of the expressiveness of their 3D bounding box outputs. This limitation was overcome by generalizing the expression of one cuboid into a collection of small cubes (voxels) that can collectively approximate arbitrary shapes by the introduction of a vision-centric 3D semantic occupancy prediction (SOP) [2] task. 3D SOP aims to capture intricate details of the surrounding scene, leveraging information derived from surrounding multi-camera images captured from different perspective views.

While previous works [23, 14, 19] emphasize the significance of temporal fusion in 3D object detection, earlier attempts at 3D SOP [16, 42, 37, 44] often overlooked the value of incorporating temporal information. This is evident in TPVFormer’s SOP visualizations, where adjacent prediction frames lack temporal semantic consistency and the frequency of false positives are high as they rely solely on the current time step for semantic predictions.

Spatial fusion lays the groundwork for temporal fusion in the context of mainstream spatial-query-based spatiotemporal transformers [23, 14, 34, 45] employing a *warp-based temporal fusion* approach. BEVFormer [23] realizes temporal fusion via the concatenation of warped history BEV features with the BEV queries, followed by temporal self-attention. Warping simply means aligning the history space according to ego-motion at the present ego-space. Scene as Occupancy [34] utilizes BEVFormer’s spatiotemporal encoder and incorporates a complex decoder to reconstruct 3D features from spatiotemporal BEV features.

We identify that CVHA can be employed for exchanging spatio-temporal information across all views. Passing information across time can be done by warping and history feature concatenation in one of the two approaches as follows: (1) Passing history only through the BEV plane, (2) Passing history through all 3 TPV planes.

However, the implementation of (1) is not simply possible. Ego pitch and roll are usually neglected as they’re not significant. When considering the yaw, the front and side views of the TPV representation at timestamp $t - 1$ could occupy different slices of the ego-space at timestamp t since the axis of the yaw is parallel to the Front and Side planes. Therefore, warping is only possible on the BEV plane. Furthermore, BEV warping is susceptible to loss of information. UniFusion [30], a spatiotemporal transformer method for map segmentation, addresses this issue by introducing *virtual views* for parallel and adaptive spatiotemporal fusion across all camera views and all time steps.

To overcome the aforementioned gaps in the 3D SOP literature, we propose **S2TPVFormer**, a unified spatiotemporal TPV encoder. We adopt TPV as the latent ego-space representation, leveraging the strengths of BEV and Voxel representations while maintaining computational efficiency. Our spatiotemporal encoder generates temporally rich S2TPV embeddings, predicting dense and

temporally coherent 3D semantic occupancy through a lightweight MLP decoder. For spatiotemporal fusion of multi-camera views onto TPV representation as introduced in (1), we first transform history camera views to the present time using Virtual View Transformation (VVT) and fuse the multi-camera features onto TPV for each time step. To enable effective interaction of features across all time steps and TPV planes, we propose Temporal Cross-View Hybrid Attention (TCVHA). This mechanism enables features to interact not only within the same time step but also across time steps, enhancing spatiotemporal context awareness and leading to a unified spatiotemporal representation. Moreover, it reduces computational complexity compared to vanilla attention mechanisms.

To summarize, this work contributes in the following ways:

- We introduce S2TPVFormer-U with a novel temporal fusion workflow for TPV representation, analyzing how CVHA facilitates the sharing of spatiotemporal information across the three planes.
- S2TPVFormer-U shows significant improvements (+4.1% mIOU) in the 3D SOP task on the nuScenes validation dataset compared to the TPVFormer.

2 Related Work

Latent 3D Scene Representations. The effectiveness of 3D scene understanding heavily relies on the representation of the 3D environment, as illustrated in Fig. 1. Traditional approaches [39, 32] involve dividing the 3D space into voxels and assigning each voxel a vector to denote its status. However, this representation proves computationally expensive. Alternatively, the Bird’s Eye View (BEV) representation, which collapses the height information and focuses on the top-down view, offers a more efficient solution. While BEV-based methods [23, 15, 6, 22, 28, 29] perform remarkably well in tasks where height information is not very important, such as 3D object detection and map segmentation, they struggle to encode the 3D structure of objects, thus hindering performance in 3D semantic occupancy prediction. Some 3D SOP methods [34] use BEV as the latent 3D scene embedding but have to employ complex decoders to reconstruct the lost height information from BEV. To overcome these limitations, TPVFormer [16] introduces a Tri-Perspective View (TPV) representation, generalizing the BEV representation by incorporating two additional orthogonal planes. In this work, we employ TPV, a hybrid explicit-implicit representation [4, 3] that aims to capture both the efficiency of BEV and the ability to encode the 3D structure of objects while being computationally efficient than the voxel representation.

2D-3D View Transformation. Transforming 2D perspective observations into 3D space latent embeddings can be considered an ill-posed problem due to the loss of depth information in 2D image formation. However, incorporating a strong *geometry prior* makes this task feasible. Monocular single-camera approaches address this challenge by predicting explicit depth maps [21, 29]. Nonetheless, depth

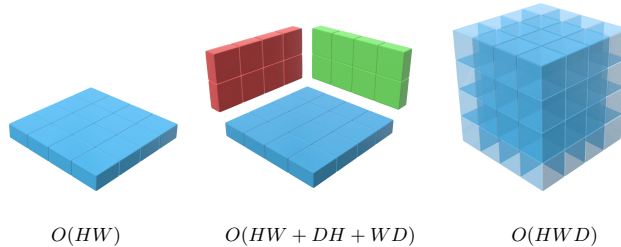


Fig. 1: Comparison of BEV, TPV [16], and Voxel latent vector fields used to represent 3D scenes. While BEV is more efficient than the Voxel representation, it discards the height information and cannot provide a holistic understanding of a 3D scene. TPV is an approach to increase efficiency without compromising the loss of height information while being in the order of the same computational complexity as BEV representation.

estimations have limitations in capturing occlusions, rendering this method sensitive to the accuracy of depth measurements.

On the other hand, LSS [29], a monocular multi-camera method proposes the LSS-based view transformation method, which first “lift”s each perspective view image individually into a frustum of feature, then “splat”s all frustums into a rasterized BEV grid. In contrast to LSS-based (depth-estimation-based) methods [22, 15], an alternative approach [16, 23, 42, 30] uses a spatial query-based approach while leveraging camera intrinsic and extrinsic parameters as a geometric prior, to fuse spatial information from 2D multi-camera perspective views into a unified latent representation for ego-space. These methods employ attention mechanisms to learn the feature fusion mapping from multi-camera latent image spaces to the unified latent ego-space representation, that aligns with spatial ego-space. This process is commonly referred to as *spatial fusion*. We adhere to the query-based view transformation since LSS-based view transformations tend to generate relatively sparse 3D representations.

Temporal Reasoning. Temporal reasoning holds equal importance to spatial reasoning in a cognitive perception system. In human perception, temporal information is crucial for identifying occluded objects and determining the motion state of entities. Spatial fusion provides a basis for temporal fusion in both warp-based temporal fusion and parallel spatiotemporal fusion. UniFusion [30] employs vanilla attention for attending to spatially mapped BEV features across all camera views and all time steps, whereas BEVFormer[23] recurrently fuses BEV features where the history features are warped to align with the ego-space of the current frame. Even though recurrent fusion can’t attend to features at all the time steps simultaneously, it is computationally efficient. The problem with warp-based temporal fusion is that, since the warping happens in ego BEV space, and ego BEV space is pre-defined to be bounded, some warped points would be mapped to points that lie out of the bounds of the original ego BEV space causing information loss. Therefore, UniFusion does the temporal alignment using

a virtual camera view mapping directly in the ego-space itself, which is prior to the ego-BEV transformation. In this paper, we combine the advantages of warp-based serial temporal fusion and parallel spatiotemporal fusion.

Vision-centric 3D Semantic Occupancy Prediction. The objective of 3D semantic occupancy prediction (*3D SOP*) is to intricately reconstruct the 3D environment surrounding an entity by incorporating detailed geometric information and semantic understanding. In the context of autonomous driving, 3D SOP serves as the academic alternative to occupancy networks [27].

MonoScene [2] is a pioneering work in vision-based 3D perception, specifically focusing on Semantic Scene Completion (SSC). It introduces the first single-camera framework for SSC, enabling the reconstruction of outdoor scenes using RGB inputs alone. Building upon the foundation of MonoScene, TPVFormer [16], the first multi-camera method for 3D Semantic Occupancy Prediction, introduces a tri-perspective view representation with a transformer-based TPV encoder. They supervise the voxel predictions using pseudo-per-voxel labels generated from the sparse point cloud by assigning a new label of *empty* to any voxel that does not contain any point. A recent line of research [37, 34, 42] argues that dense semantic occupancy predictions require dense labels, and they propose pipelines to generate densified ground-truth voxel semantics. OcFormer [44] introduces a dual-path transformer to efficiently process the 3D volume and achieve long-range occupancy prediction. FB-OCC [24] proposes a forward-backward view transformation to combine the advantages of LSS-based and query-based view transformation.

3 Methodology

3.1 Overall Architecture

Our S2TPVFormer pipeline consists of four major modules: (1) an image backbone to extract 2D multi-scale features, (2) a spatiotemporal TPV encoder for generating spatiotemporal 3D semantic occupancy embeddings (which we will call S2TPV features), (3) a simple feature aggregator that broadcasts each S2TPV plane along the corresponding perpendicular axis and sums them to generate voxel features, and (4) a lightweight MLP head for predicting the semantic labels of individual voxels.

3.2 Image Backbone

The image backbone consists of two networks: a feature extractor network and a neck module to extract multi-scale features, for granularity. The image backbone network extracts multi-scale features for all the input surrounding multi-camera images at a time and provides the foundation for the S2TPV encoder. We employ a ResNet [12] as the image feature extractor and an FPN [25] to produce multi-scale features. With the N_{cam} number of surround multi-camera images, \mathbf{I}_t , received at the time step t , the image backbone is used to extract multi-level 2D perspective view features for each camera view. We denote

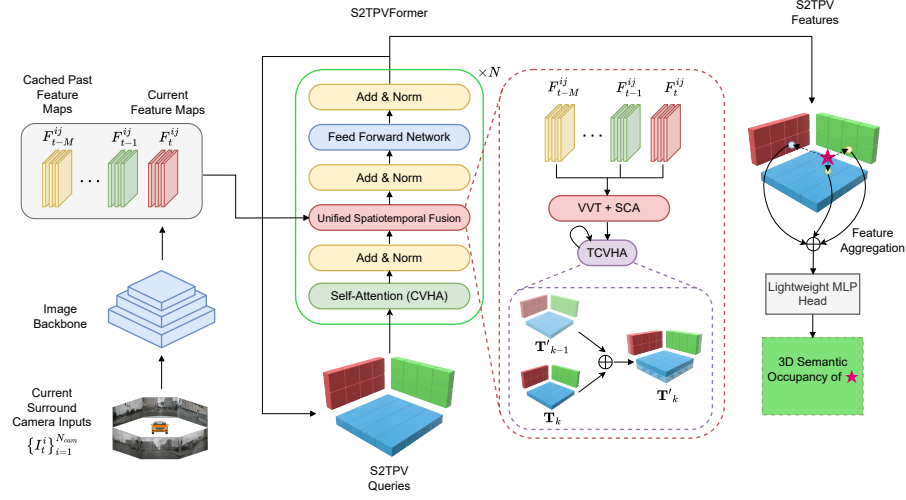


Fig. 2: The 3D SOP pipeline for the proposed S2TPVFormer architecture.

these as $\mathbf{F}_t = \{\{F_t^{ij}\}_{j=1}^{N_{scale}}\}_{i=1}^{N_{cam}}$. Since the proposed the pipeline is not limited to a specific image backbone, it can be replaced with any other feature extractor network such as ViT [9], or SwinTransformer [26] along with any FPN variant such as BiFPN [36] or NAS-FPN [11].

3.3 Spatio-Temporal TPV Encoder

We provide two variants of S2TPVFormer based on the type of temporal fusion. The S2TPVFormer-U encoder, which is our main contribution, consists of three major components, which are, (1) the S2TPV queries, (2) the Self-Attention module, and (3) the Unified Spatiotemporal Fusion module, as illustrated in Fig. 2.

During inference, we cache these features in a queue for each time step. These history feature maps along with the current feature maps, $\{\mathbf{F}_{t-k}^{ij}\}_{k=0}^M$ where M is the total number of temporal fusion steps, are fed to the Unified Spatiotemporal Fusion module of our S2TPVFormer encoder to fuse features across all camera views and time steps onto the S2TPV queries. Essentially, this module does the following, (1) Virtual View Transformation (VVT) to view camera features as if they were present in the current time step, followed by Spatial Cross Attention (SCA) to fuse virtual camera view features onto S2TPV queries for each time step, and (2) Fuse the virtual spatial TPV features across all time steps via TCVHA. The temporal fusion in Temporal Cross-View Hybrid Attention (TCVHA), that we introduce extending CVHA, is realized via the concatenation of previous S2TPV features with current spatial TPV features as shown below the TCVHA module. A separate CVHA module is used to self attend to S2TPV features to refine the queries and produce temporally coherent

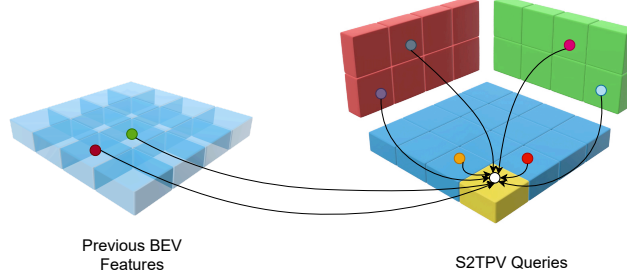


Fig. 3: TCVHA Spatiotemporal Interactions. For a given BEV query feature q at a point $p = (h, w)$, it interacts with four types of feature points: (1) history points, (2) self points, (3) front viewpoints, and (4) side viewpoints. Temporal fusion is realized via the interactions with the history points. This diagram does not show the interactions with previous front and side view features.

semantic occupancy embeddings. The S2TPV occupancy embeddings are finally aggregated and fed through a lightweight MLP head.

S2TPVFormer-W encoder on the other hand employs warp-based recurrent temporal fusion using TCVHA in place of the self-attention module and Spatial Cross-Attention (SCA) module in place of the Unified Spatiotemporal Module to lift 2D scene features to 3D and fuse them onto S2TPV queries. In S2TPVFormer-W, the BEV features of the S2TPV features computed at the previous time step are preserved and warped according to the ego-motion following BEVFormer [23] to be temporally fused via TCVHA with the current S2TPV queries. Even though the direct temporal fusion via concatenation is done on the BEV plane, TCVHA allows interactions between all three planes in the current queries as well as in the previous BEV features as shown in Fig. 3.

Unified Spatiotemporal Fusion. This is the most crucial component of the S2TPVFormer-U. Since the spatial and temporal fusion in S2TPVFormer-U happens parallelly, the spatial alignment of the history frames has to be done across the camera views in the current ego space. To achieve this, given a past time frame, we use the VVT, as expressed in Eq. (1) and (2). In these equations, $R_i^{v,p}$ and $t_i^{v,p}$ are the rotation and the translation of the virtual view transformation for the p^{th} time step, R_i and t_i are the camera sensor to ego-space rotation and translation of the i^{th} camera, R_c and t_c are the ego-space to global coordinate transformation for the current time step, and R_p and t_p are the ego-space to global coordinate transformation for the past time step. $R_i^{v,p}$ and $t_i^{v,p}$ altogether view an ego-space point in a past time step as if it is present in the current time step (a virtual point), in the perspective of the i^{th} camera sensor.

$$R_i^{v,p} = R_i^{-1} R_p^{-1} R_c \quad (1)$$

$$t_i^{v,p} = R_i^{-1} R_p^{-1} t_c - R_i^{-1} R_p^{-1} t_p - R_i^{-1} t_i \quad (2)$$

We implement spatial fusion using 3D Deformable Attention [23] to save the computational burden of using vanilla attention because of the high number of

S2TPV query and multi-scale-multi-camera key interactions. After the VVT, the 2D camera view feature queue is fed through the Spatial Cross-Attention (SCA) module to lift those into the current ego 3D TPV space. The actual virtual camera feature mapping is done using the camera intrinsic and the VVT, to derive the reference points expressed in Eq. (4) for the deformable attention. For a S2TPV query $q_{h,w} \in Q^{HW}$ located at (h, w) , we uniformly sample N_{ref}^{HW} reference points along the orthogonal direction [18] of the plane as described in Eq. (3). These points are then transformed using the VVT and camera intrinsic which provides the geometry prior to the 2D-3D lifting, to get the final virtual image reference points. For the attention-based fusion, only the views that the projected reference point, $\mathbf{Ref}_{h,w}^{v,i}$, hits within the image are considered to further improve the computational efficiency. The SCA function that does the actual spatial fusion is described in Eq. (5).

$$\mathbf{Ref}_{h,w}^{ego} = \{(h, w, d_k)\}_{k=1}^{N_{ref}^{HW}} \quad (3)$$

$$\mathbf{Ref}_{h,w}^{v,i} = K_i R_i^{v,p} \mathbf{Ref}_{h,w}^{ego} + t_i^{v,p} \quad (4)$$

$$\text{SCA}(q_{h,w}, \mathbf{F}_t) = \frac{1}{|V_{hit}|} \sum_{i \in V_{hit}} \text{3DDeformAttn}(q_{h,w}, \mathbf{Ref}_{h,w}^{v,i}, \mathbf{F}_t^i) \quad (5)$$

In Eq. (3) and (4), $\mathbf{Ref}_{h,w}^{ego}$ are the reference points generated in the ego-TPV space for each TPV plane, $\mathbf{Ref}_{h,w}^{v,i}$ are the i^{th} virtual camera view reference points for 3D deformable attention, and K_i is the camera intrinsic of the i^{th} camera sensor. In Eq. (5), V_{hit} denotes the set of hit camera views. Note that the above formulations are only considering the Q^{HW} query plane. These computations will be the same for the other two planes. After spatial cross-attention, the resulting features are $\mathbf{T}_t = T_t^{HW} \cup T_t^{DH} \cup T_t^{WD}$.

Temporal Cross-View Hybrid Attention. Realizing the capability of CVHA in self-attending to S2TPV representation, we construct TCVHA, essentially for CVHA to interact with history S2TPV features as well. As depicted in Fig. 3, these interactions allow the S2TPV queries to enhance the spatiotemporal context further by filtering out irrelevancies by attending to both the current S2TPV queries and prior S2TPV features. Fig. 2 illustrates the recurrent style temporal fusion of TCVHA more clearly below the TCVHA block. Given the spatially fused TPV features \mathbf{T}_t for all the time steps in the history queue, the queries for the TCVHA are created iteratively as given in Eq. (6), (7) and (8), where $q'_{k,h,w} \in \mathbf{Q}'_k$ are the queries for the TCVHA operation at k^{th} iteration, and $\{\cdot\}$ represents the concatenation operation. For the first iteration, \mathbf{T}_{t-M} (spatially fused TPV features of the last temporal fusion step) is concatenated with itself.

Here, the intermediate S2TPV features at $(k-1)^{th}$ iteration act as the warped previous features that are concatenated with queries in warp-based serial temporal fusion [23]. The cross-view reference points, $\mathbf{Ref}_{h,w}^{cross}$, are generated in the same way as in [16]. Using these intermediate features as queries, TCVHA computes the temporally fused intermediate S2TPV features at k^{th} iteration as

expressed in Eq. (8). This is recursively repeated for M number of temporal fusion steps until we get the final unified spatiotemporal features \mathbf{T}'_t .

$$\mathbf{Q}'_k = \{T'^{HW}_{k-1}, T_k^{HW}\} \cup \{T'^{DH}_{k-1}, T_k^{DH}\} \cup \{T'^{WD}_{k-1}, T_k^{WD}\} \quad (6)$$

$$\text{TCVHA}(q'_{k,h,w}) = \text{DeformAttn}(q'_{k,h,w}, \mathbf{Ref}_{h,w}^{cross}, \mathbf{T}'_k) \quad (7)$$

$$\mathbf{T}'_k = \text{TCVHA}(q'_{k,h,w}) \quad (8)$$

4 Experimental Setup and Implementation

4.1 Datasets and Evaluation Metrics

nuScenes [10] is a large-scale dataset for autonomous driving research, providing 1000 urban driving scenes with annotations for object detection. It includes diverse weather conditions, times of day, and urban environments across Boston, Singapore, Pittsburgh, and Las Vegas. The dataset contains 28,130 training and 6,018 validation keyframes, captured at 20Hz. It incorporates data from monocular cameras, LiDAR, RADAR, and GPS, with 1.1 billion LiDAR points manually annotated for 32 classes.

For 3D perception tasks such as *LiDAR Segmentation* and *3D SOP*, mean Intersection over Union (mIoU) stands as a significant validation metric to measure model accuracy. IoU measures the overlap between predicted and ground truth bounding boxes or segmented regions, offering a precise assessment of localization accuracy. A higher IoU signifies better alignment between predicted and actual boundaries. Complementing this, mIoU calculates the average IoU across multiple classes, providing an overall performance indicator.

4.2 Training for 3D Semantic Occupancy Prediction and LiDAR Segmentation

Ground Truth Labels for Supervision: Models for both 3D SOP and LiDAR segmentation are trained with supervision from the training set of the nuScenes dataset. The nuScenes dataset comprises images, sparse LiDAR points from sweeps across the scene, and annotations of the 16 semantic classes for each point. To train our models, we divide the 3D space into a voxel grid and assign the semantic label of the LiDAR points that fall into a voxel as the semantic label of the voxel itself. A new semantic class, "empty," is assigned to all voxels without any LiDAR points falling onto them for training the 3D SOP model. This approach is in line with the standard practices proposed in various studies (referenced as [16, 42, 44, 37]). It should be noted that we do not generate super-resolution voxel semantic labels, as has been done in some parallel work (cited as [37, 42]).

Loss Functions: We use two loss functions for supervision during training: (a) a Cross-entropy loss to improve voxel classification accuracy and (b) a Lovasz-softmax loss [1] to maximize the IoU score across classes. When training for

Table 1: Model configurations used to run experiments

| Model Config | Embedding Dimensionality | TPV Resolution | Backbone | Image Resolution |
|-------------------|-----------------------------|-------------------|-----------|---------------------|
| S2TPVFormer-base | 256 | 100x100x8 | ResNet101 | 1600x900 |
| S2TPVFormer-small | 128 | 100x100x8 | ResNet50 | 1600x900 |

3D SOP (3D Semantic Object Parsing), we supervise our voxel predictions using the Lovasz loss and the LiDAR point queried output using Cross-entropy loss. Following the result in the ablation study by TPVFormer [16] for **LiDAR Segmentation**, we use voxel predictions as input for Cross-entropy loss, and point predictions as input for Lovasz-softmax loss to achieve the best mean IoU (mIoU). This approach not only enables the model to generate point predictions but also assists the latent representation in learning the discretization strategy inherent in voxel space.

Training: We train our models on 4 NVIDIA A6000 GPUs with 48G capacity. We use a batch size of 1 per GPU. AdamW [17] optimizer was employed over 24 epochs, initiating with a learning rate of 2×10^{-4} , which was then adjusted according to a cosine annealing schedule. We have used several data augmentation techniques, including image scaling, color distortion, and Gridmask [5].

4.3 Implementation Details

We implement two versions of S2TPVFormer, as discussed in Section 3.3, which differ based on the method of temporal fusion and the level of interaction among the three TPV planes in the latent representation of the encoder. Both versions utilize the same decoder head, a lightweight MLP consisting of two linear layers with an intermediate Softplus activation layer. This decoder is applied to voxel features to predict their semantic labels, emphasizing the encoder’s efficiency by opting for a lightweight MLP over a more complex decoder. For different configurations defined in Table 1, S2TPVFormer-base employs the ResNet101-DCN [7] initialized from an FCOS3D [38] checkpoint. In contrast, another version (which needs a distinct name for clarification) uses ResNet50 [12] pre-trained on the ImageNet dataset [8].

5 Results and Analysis

5.1 Analysis of 3D Semantic Occupancy Prediction Results

Quantitative Analysis: The experimental results demonstrate that S2TPVFormer outperforms the TPVFormer baseline in 3D Semantic Object Parsing (SOP). As shown in Table 2, we achieve a 4.1% improvement over TPVFormer for SOP. This highlights the contribution of our temporal attention mechanism. It is also noteworthy that the IoU increases for fourteen out of the sixteen classes, demonstrating the robustness of the proposed methodology.

Table 2: 3D Semantic Occupancy Prediction results on the nuScenes validation set. It is fair to compare the results of TPVFormer and S2TPVFormer-U (Base) as our Base configuration is the same as the configuration TPVFormer has used for 3D SOP.

| Method | mIoU (%) | barrier | bicycle | bus | car | const. veh. | motorcycle | pedestrian | traffic cone | trailer | truck | drive. surf. | other flat | sidewalk | terrain | manmade | vegetation |
|-----------------------|-------------|-------------|-------------|-------------|-------------|-------------|-------------|-------------|--------------|-------------|-------------|--------------|-------------|-------------|-------------|-------------|-------------|
| TPVFormer [16] | 52.0 | 59.6 | 26.3 | 77.6 | 74.1 | 30.9 | 47.5 | 41.8 | 20.2 | 44.9 | 67.8 | 86.3 | 54.5 | 55.5 | 54.6 | 47.5 | 44.0 |
| S2TPVFormer-U (Base) | 56.1 | 60.1 | 16.5 | 85.9 | 74.3 | 42.2 | 51.5 | <u>37.0</u> | 21.2 | 49.4 | 74.2 | 86.4 | 56.3 | 57.9 | 55.0 | 65.4 | 65.0 |
| S2TPVFormer-U (Small) | 43.4 | 54.3 | <u>17.2</u> | 66.0 | 69.5 | 28.2 | 22.8 | 32.1 | 15.1 | 31.7 | 59.6 | 82.4 | 49.9 | 47.8 | 47.4 | 34.9 | 36.0 |

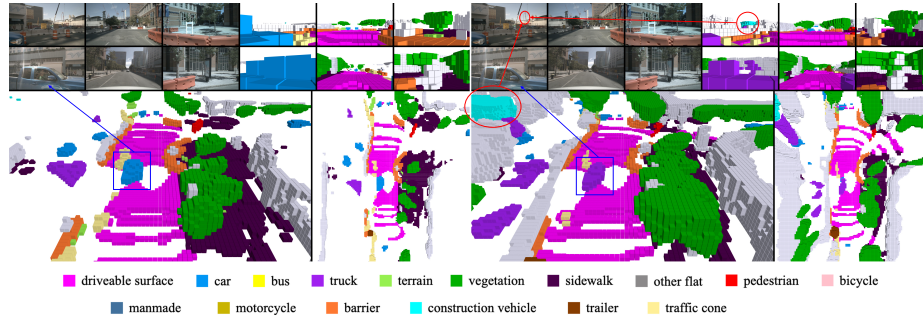


Fig. 4: Qualitative results on nuScenes validation set. TPVFormer’s predictions are visualized on the left side, and S2TPVFormer’s predictions are on the right side.

Qualitative Analysis: In Fig. 4, we illustrate the model’s capability to predict 3D semantic occupancy surrounding the ego vehicle. This figure presents six input camera images fed into the model, alongside eight representations of the semantic occupancy predictions made by the model for the same frame from the nuScene validation set. Through a comparative study with TPVFormer, we highlight the enhancements achieved through our novel temporal attention module.

Our analysis particularly focuses on two critical objects identified in the camera images for this frame; (a) a truck passing closely by the ego vehicle on its left, highlighted with a blue circle. TPVFormer misclassifies this truck as a car, which we believe is due to the truck’s proximity to the ego vehicle, resulting in only the top half of the truck being visible in the camera image, thus resembling a car. Conversely, S2TPVFormer-U accurately identifies it as a truck. We argue that this accuracy stems from the model’s ability to integrate information from preceding frames, where the truck is captured in full from a distance, allowing the temporal fusion capability of S2TPVFormer-U to effectively utilize past frame data for accurate prediction. (b) A construction vehicle (more specifically a crane), highlighted with a red circle, visible in the distance in the front-left camera image. TPVFormer fails to recognize this object, predicting the space

as empty, whereas S2TPVFormer-U successfully detects the construction vehicle’s presence. We contend that the model’s access to temporally enriched image features enables S2TPVFormer-U to identify distant objects such as this.

Another notable observation from our analysis is the density of the predictions generated by S2TPVFormer-U are significantly denser than those by TPVFormer, even when both models are trained on the same nuScenes dataset, which has sparse ground truth.

5.2 Analysis of LiDAR Segmentation Results

We test the performance of S2TPVFormer-U (base) for LiDAR segmentation to assess the generalization capabilities of our model, with a particular focus on the novel temporal attention module in S2TPVFormer. We report the results of LiDAR segmentation on the nuScenes test and validation sets in Table 3 and Table 4, respectively. In Table 3, we include results for some of the best-performing methods in the nuScenes LiDAR segmentation challenge, covering both models that use cameras and those that use LiDAR as the input modality. Even after training for only four epochs, our model achieves results that are comparable with state-of-the-art methods in the literature.

Table 3: LiDAR Segmentation performance on the nuScenes test set. * represents the produced upon completion of training over four epochs. † represents that TPVFormer-Small and TPVFormer-Base are different from S2TPVFormer-Small and S2TPVFormer-Base

| Method | Input Modality | mIoU | barrier | bicycle | bus | car | const. veh. | motorcycle | pedestrian | traffic cone | trailer | truck | drive. surf. | other flat | sidewalk | terrain | manmade | vegetation |
|-----------------------|----------------|------|---------|---------|------|------|-------------|------------|------------|--------------|---------|-------|--------------|------------|----------|---------|---------|------------|
| MINet [20] | LiDAR | 56.3 | 54.6 | 8.2 | 62.1 | 76.6 | 23.0 | 58.7 | 37.6 | 34.9 | 61.5 | 46.9 | 93.3 | 56.4 | 63.8 | 64.8 | 79.3 | 78.3 |
| LidarMultiNet [43] | LiDAR | 81.4 | 80.4 | 48.4 | 94.3 | 90.0 | 71.5 | 87.2 | 85.2 | 80.4 | 86.9 | 74.8 | 97.8 | 67.3 | 80.7 | 76.5 | 92.1 | 89.6 |
| UniVision [13] | LiDAR | 72.3 | 72.1 | 34.0 | 85.5 | 89.5 | 59.3 | 75.5 | 69.3 | 65.8 | 84.2 | 71.4 | 96.1 | 67.4 | 71.9 | 65 | 77.9 | 71.7 |
| PanoOcc [41] | LiDAR | 71.4 | 82.5 | 32.3 | 88.1 | 83.7 | 46.1 | 76.5 | 67.6 | 53.6 | 82.9 | 69.5 | 96.0 | 66.3 | 72.3 | 66.3 | 80.5 | 77.3 |
| OccFormer [44] | LiDAR | 70.8 | 72.8 | 29.9 | 87.9 | 85.6 | 57.1 | 74.9 | 63.2 | 53.5 | 83 | 67.6 | 94.8 | 61.9 | 70.0 | 66.0 | 84.0 | 80.5 |
| TPVFormer-Small† [16] | Camera | 59.2 | 65.6 | 15.7 | 75.1 | 80.0 | 45.8 | 43.1 | 44.3 | 26.8 | 72.8 | 55.9 | 92.3 | 53.7 | 61.0 | 59.2 | 79.7 | 75.6 |
| TPVFormer-Base† [16] | Camera | 69.4 | 74.0 | 27.5 | 86.3 | 85.5 | 60.7 | 68.0 | 62.1 | 49.1 | 81.9 | 68.4 | 94.1 | 59.5 | 66.5 | 63.5 | 83.8 | 79.9 |
| S2TPVFormer-U (Base)* | Camera | 60.4 | 61.2 | 18.2 | 80.6 | 78.1 | 55.2 | 57.6 | 41.5 | 26.4 | 76.1 | 61.3 | 89.8 | 49.4 | 56.6 | 58.0 | 79.3 | 76.4 |

5.3 Ablation Study

We carry out two main ablation studies for 3D Semantic Object Parsing (SOP) to understand the effects of: (a) the range of temporal attention during inference, and (b) the dimensionality of S2TPV embedding, on the ability of our temporal attention module to support the task of 3D SOP.

Table 4: LiDAR Segmentation results on nuScenes validation set. * represents the produced upon completion of training over four epochs. † represents that TPVFormer-Small and TPVFormer-Base are different from S2TPVFormer-Small and S2TPVFormer-Base

| Method | Input Modality | mIoU | barrier | bicycle | bus | car | const. veh. | motorcycle | pedestrian | traffic cone | trailer | truck | drive. surf. | other flat | sidewalk | terrain | manmade | vegetation |
|-----------------------|----------------|------|---------|---------|------|------|-------------|------------|------------|--------------|---------|-------|--------------|------------|----------|---------|---------|------------|
| BEVFormer [23] | Camera | 56.2 | 54.0 | 22.8 | 76.7 | 74.0 | 45.8 | 53.1 | 44.5 | 24.7 | 54.7 | 65.5 | 88.5 | 58.1 | 50.5 | 52.8 | 71.0 | 63.0 |
| TPVFormer-Base [16]† | Camera | 68.9 | 70.0 | 40.9 | 93.7 | 85.6 | 49.8 | 68.4 | 59.7 | 38.2 | 65.3 | 83.0 | 93.3 | 64.4 | 64.3 | 64.5 | 81.6 | 79.3 |
| TPVFormer-Small [16]† | Camera | 59.3 | 64.9 | 27.0 | 83.0 | 82.8 | 38.3 | 27.4 | 44.9 | 24.0 | 55.4 | 73.6 | 91.7 | 60.7 | 59.8 | 61.1 | 78.2 | 76.5 |
| S2TPVFormer-U (base) | Camera | 61.6 | 62.9 | 25.5 | 87.4 | 81.3 | 51.6 | 64.2 | 45.7 | 22.0 | 57.4 | 77.5 | 89.3 | 50.4 | 56.5 | 58.9 | 78.7 | 76.4 |

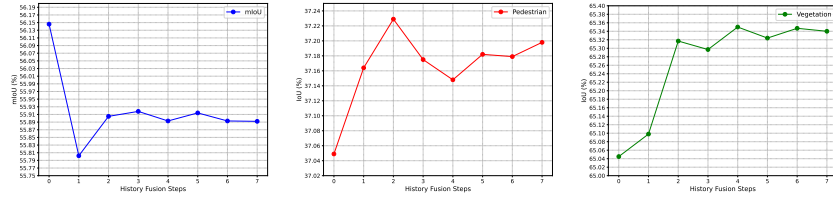


Fig. 5: Potential of long-range temporal fusion.

Range of temporal attention: As discussed in Sec. 3.3, the training of our S2TPVFormer-U model is conducted using a single previous time frame for temporal attention. This study aims to examine the variation in performance for 3D Semantic Occupancy Prediction (SOP) as a function of varying extents of temporal attention during the inference process. It is important to note that we change the history fusion steps only for inference.

As depicted in Figure 5, we present an analysis utilizing eight distinct temporal history fusion steps within the context of temporal attention, examining their impact across two semantic classes as well as on the mean Intersection over Union (mIoU). It is observed that the optimal number of history fusion steps necessary to achieve the most favorable outcomes differs among the semantic classes. This observation underscores the inherent potential for temporal fusion within our model, although it remains underexploited at the current juncture.

S2TPV embedding dimensionality: We train our S2TPVFormer-U and our implementation of TPVFormer (referred to as TPVFormer-Small* in Table 5) under the S2TPVFormer-Small configuration, as defined in Tab. 1. From the mIoU scores presented in Tab. 5, we can draw two important observations: (a) the mIoU scores of both TPVFormer and S2TPVFormer-U increase with the enhancement of embedding dimensionality, and (b) TPVFormer* attains a higher mIoU than S2TPVFormer-U in the Small configuration, even though the opposite is true for the Base configuration. These observations lead us to conclude that (a) a higher embedding dimensionality indeed facilitates the TPV repre-

Table 5: Summary of the ablation study on embedding dimensionality. The objective is to demonstrate the effect of embedding dimensionality on the performance of temporal attention. * represents the reproduced results using our implementation of the TPVFormer’s architecture.

| Ablation | mIoU (%) |
|-----------------------|-------------|
| TPVFormer-Small* | 44.4 |
| S2TPVFormer-U (Small) | 43.4 |
| TPVFormer | 52.0 |
| S2TPVFormer-U (Base) | 55.0 |

sensation’s ability to learn and retain the additional information it receives via temporal attention, and (b) our model demonstrates promising scalability when compared to TPVFormer.

6 Conclusion

In this paper, we delve into the potential of exploiting spatiotemporal intricacies in the TPV representation to enhance the temporal coherence of 3D Semantic Occupancy Prediction within the existing TPVFormer architecture. We are pioneers in implementing this enhancement, aiming to elevate the model’s ability to understand the 3D scene over time. Leveraging 2D-3D spatial cross-attention, we lift multi-camera scene features to 3D scene features, forming the groundwork for effective temporal fusion across TPV planes. With the support of Cross-View Hybrid Attention, this approach significantly advances the TPVFormer’s present performance in 3D perception.

The obvious use case of the proposed system is the realization of fully automated self-driving. The authors intend to stress the importance of training and testing the proposed system on a larger and more diverse dataset prior to any real-world application. The results presented in this paper are biased by the geographic limitations of data collection, quality of equipment and the distribution of roadside views. Furthermore, the reported metrics such as mIoU are a gross oversimplification of the actual parameters required to assess a system for real-world deployment. We hope our work will inspire a line of work to handle these concerns.

Our work is an important step in the bigger journey of achieving accurate 3D vision. We have exhibited the advantage of utilizing temporal information to improve the accuracy in both 3D SOP and LiDAR Segmentation. However, we are yet to see the full utility of long-range temporal information passing in these problem domains. Another interesting avenue of exploration would be how our proposed methodology improves with dense semantic captions.

References

- [1] Maxim Berman, Amal Rannen Triki, and Matthew B Blaschko. “The lovász-softmax loss: A tractable surrogate for the optimization of the intersection-over-union measure in neural networks”. In: *Proceedings of the IEEE conference on computer vision and pattern recognition*. 2018, pp. 4413–4421.
- [2] Anh-Quan Cao and Raoul de Charette. “MonoScene: Monocular 3D Semantic Scene Completion”. In: *CVPR*. 2022.
- [3] Eric R. Chan et al. “Efficient Geometry-aware 3D Generative Adversarial Networks”. In: 2022.
- [4] Anpei Chen et al. “TensorRF: Tensorial Radiance Fields”. In: 2022.
- [5] Pengguang Chen et al. *GridMask Data Augmentation*. 2020. DOI: [10.48550/ARXIV.2001.04086](https://doi.org/10.48550/ARXIV.2001.04086). URL: <https://arxiv.org/abs/2001.04086>.
- [6] Kashyap Chitta, Aditya Prakash, and Andreas Geiger. “NEAT: Neural Attention Fields for End-to-End Autonomous Driving”. In: *International Conference on Computer Vision (ICCV)*. 2021.
- [7] Jifeng Dai et al. “Deformable Convolutional Networks”. In: *Proceedings of the IEEE International Conference on Computer Vision (ICCV)*. Oct. 2017.
- [8] Jia Deng et al. “Imagenet: A large-scale hierarchical image database”. In: *2009 IEEE conference on computer vision and pattern recognition*. Ieee. 2009, pp. 248–255.
- [9] Alexey Dosovitskiy et al. *An Image is Worth 16x16 Words: Transformers for Image Recognition at Scale*. 2021. arXiv: [2010.11929](https://arxiv.org/abs/2010.11929) [cs.CV].
- [10] Whye Kit Fong et al. “Panoptic nuScenes: A Large-Scale Benchmark for LiDAR Panoptic Segmentation and Tracking”. In: *arXiv preprint arXiv:2109.03805* (2021).
- [11] Golnaz Ghiasi et al. *NAS-FPN: Learning Scalable Feature Pyramid Architecture for Object Detection*. 2019. arXiv: [1904.07392](https://arxiv.org/abs/1904.07392) [cs.CV].
- [12] Kaiming He et al. “Deep residual learning for image recognition”. In: *Proceedings of the IEEE conference on computer vision and pattern recognition*. 2016, pp. 770–778.
- [13] Yu Hong et al. “UniVision: A Unified Framework for Vision-Centric 3D Perception”. In: (Jan. 2024). arXiv: [2401.06994](https://arxiv.org/abs/2401.06994) [cs.CV].
- [14] Junjie Huang and Guan Huang. “BEVDet4D: Exploit Temporal Cues in Multi-camera 3D Object Detection”. In: *arXiv preprint arXiv:2203.17054* (2022).
- [15] Junjie Huang et al. “BEVDet: High-performance multi-camera 3D object detection in Bird-Eye-View”. In: (Dec. 2021).
- [16] Yuanhui Huang et al. “Tri-Perspective View for Vision-Based 3D Semantic Occupancy Prediction”. In: 2023.
- [17] Diederik P Kingma and Jimmy Ba. “Adam: A method for stochastic optimization”. In: (2014).
- [18] Alex H. Lang et al. “PointPillars: Fast Encoders for Object Detection from Point Clouds”. In: 2019.

- [19] Qi Li et al. *HDMaPNet: An Online HD Map Construction and Evaluation Framework*. 2021.
- [20] Shijie Li et al. “Multi-Scale Interaction for Real-Time LiDAR Data Segmentation on an Embedded Platform”. In: *IEEE Robotics and Automation Letters* 7.2 (2022), pp. 738–745. DOI: [10.1109/LRA.2021.3132059](https://doi.org/10.1109/LRA.2021.3132059).
- [21] Yiming Li et al. “VoxFormer: Sparse Voxel Transformer for Camera-based 3D Semantic Scene Completion”. In: 2023.
- [22] Yinhao Li et al. “BEVDepth: Acquisition of reliable depth for multi-view 3D object detection”. In: (June 2022).
- [23] Zhiqi Li et al. “BEVFormer: Learning bird’s-eye-view representation from multi-camera images via spatiotemporal transformers”. In: (Mar. 2022).
- [24] Zhiqi Li et al. *FB-OCC: 3D Occupancy Prediction based on Forward-Backward View Transformation*. 2023. arXiv: [2307.01492](https://arxiv.org/abs/2307.01492) [[cs.CV](#)].
- [25] Tsung-Yi Lin et al. *Feature Pyramid Networks for Object Detection*. 2017. arXiv: [1612.03144](https://arxiv.org/abs/1612.03144) [[cs.CV](#)].
- [26] Ze Liu et al. “Swin Transformer: Hierarchical Vision Transformer using Shifted Windows”. In: 2021.
- [27] Lars Mescheder et al. *Occupancy Networks: Learning 3D Reconstruction in Function Space*. 2019.
- [28] Chen Min et al. “Occ-BEV: Multi-Camera Unified Pre-training via 3D Scene Reconstruction”. In: 2023.
- [29] Jonah Philion and Sanja Fidler. “Lift, splat, shoot: Encoding images from arbitrary camera rigs by implicitly unprojecting to 3D”. In: (Aug. 2020).
- [30] Zequn Qin et al. “UniFusion: Unified multi-view fusion transformer for spatial-temporal representation in bird’s-eye-view”. In: (July 2022).
- [31] Luis Roldão, Raoul de Charette, and Anne Verroust-Blondet. “LMSCNet: Lightweight Multiscale 3D Semantic Completion”. In: (Aug. 2020).
- [32] Danila Rukhovich, Anna Vorontsova, and Anton Konushin. “ImVoxelNet: Image to Voxels Projection for Monocular and Multi-View General-Purpose 3D Object Detection”. In: 2021.
- [33] Shaoshuai Shi, Xiaogang Wang, and Hongsheng Li. “PointRCNN: 3D object proposal generation and detection from point cloud”. In: (Dec. 2018).
- [34] Chonghao Sima et al. “Scene as Occupancy”. In: (2023).
- [35] Andrea Simonelli et al. “Disentangling monocular 3D object detection”. In: (May 2019).
- [36] Mingxing Tan, Ruoming Pang, and Quoc V. Le. *EfficientDet: Scalable and Efficient Object Detection*. 2020. arXiv: [1911.09070](https://arxiv.org/abs/1911.09070) [[cs.CV](#)].
- [37] Xiaoyu Tian et al. “Occ3D: A Large-Scale 3D Occupancy Prediction Benchmark for Autonomous Driving”. In: *arXiv preprint arXiv:2304.14365* (2023).
- [38] Tai Wang et al. “FCOS3D: Fully convolutional one-stage monocular 3D object detection”. In: (Apr. 2021).
- [39] Yan Wang et al. “Pseudo-LiDAR from Visual Depth Estimation: Bridging the Gap in 3D Object Detection for Autonomous Driving”. In: 2020.
- [40] Yue Wang et al. “DETR3D: 3D Object Detection from Multi-view Images via 3D-to-2D Queries”. In: (Oct. 2021).

- [41] Yuqi Wang et al. “PanoOcc: Unified occupancy representation for camera-based 3D panoptic segmentation”. In: (June 2023). arXiv: [2306.10013 \[cs.CV\]](#).
- [42] Yi Wei et al. “SurroundOcc: Multi-Camera 3D Occupancy Prediction for Autonomous Driving”. In: 2023.
- [43] Dongqiangzi Ye et al. “LidarMultiNet: Towards a Unified Multi-Task Network for LiDAR Perception”. In: *Proceedings of the AAAI Conference on Artificial Intelligence* 37.3 (June 2023), pp. 3231–3240. DOI: [10.1609/aaai.v37i3.25429](#). URL: <https://ojs.aaai.org/index.php/AAAI/article/view/25429>.
- [44] Yunpeng Zhang, Zheng Zhu, and Dalong Du. “OccFormer: Dual-path transformer for vision-based 3D semantic occupancy prediction”. In: (Apr. 2023). arXiv: [2304.05316 \[cs.CV\]](#).
- [45] Yunpeng Zhang et al. “BEVerse: Unified Perception and Prediction in Birds-Eye-View for Vision-Centric Autonomous Driving”. In: 2022.
- [46] Xinge Zhu et al. “Cylindrical and asymmetrical 3D convolution networks for LiDAR-based perception”. In: (Sept. 2021).